BIOCHEMISTRY
including biophysical chemistry & molecular biology
Article

Biochemistry **2011,** *50,* 763–769 763
DOI: 10.1021/bi101375d

Role for a Conserved Structural Motif in Assembly of a Class I Aminoacyl-tRNA Synthetase Active Site†

Veronica C. Casina, Andrew A. Lobashevsky, William E. McKinney, Cassidy L. Brown, and Rebecca W. Alexander*

Department of Chemistry, Wake Forest University, Winston-Salem, North Carolina 27109-7486, United States

Received August 25, 2010; Revised Manuscript Received December 14, 2010

ABSTRACT: The catalytic domains of class I aminoacyl-tRNA synthetases are built around a conserved Rossmann nucleotide binding fold, with additional polypeptide domains responsible for tRNA binding or hydrolytic editing of misacylated substrates. Structural comparisons identified a conserved motif bridging the catalytic and anticodon binding domains of class Ia and Ib enzymes. This stem contact fold (SCF) has been proposed to globally orient each enzyme's cognate tRNA by interacting with the inner corner of the L-shaped tRNA. Despite the structural similarity of the SCF among class Ia/Ib enzymes, the sequence conservation is low. We replaced amino acids of the MetRS SCF with portions of the structurally similar glutaminyl-tRNA synthetase (GlnRS) motif or with alanine residues. Chimeric variants retained significant tRNA methionylation activity, indicating that structural integrity of the helix−turn−strand−helix motif contributes more to tRNA aminoacylation than does amino acid identity. In contrast, chimeras were significantly reduced in methionyl adenylate synthesis, suggesting a role for the SCF in formation of a structured active site domain. A highly conserved aspartic acid within the MetRS SCF is proposed to make an electrostatic interaction with an active site lysine; these residues were replaced with alanines or conservative substitutions. Both methionyl adenylate formation and methionine transfer were impaired, and activity was not significantly recovered by making the compensatory double substitution.

Aminoacyl-tRNA synthetases (aaRSs) catalyze the attachment of amino acids to their cognate tRNAs, thereby establishing and maintaining the genetic code (*1*). The 20 aaRSs are partitioned into two classes of ten enzymes each based on sequence and structural similarities in their catalytic domains (*2*, *3*). The catalytic domain binds amino acid and ATP substrates, catalyzes formation of the activated aminoacyl adenylate, and transfers the amino acid to an isoaccepting tRNA. The tRNA aminoacylation reaction occurs in two enzyme-catalyzed steps for both classes of aaRSs:

$$\mathrm{AA} + \mathrm{ATP} + \mathrm{aaRS} \leftrightarrow \mathrm{aaRS \cdot AA\text{-}AMP} + \mathrm{PP_i}\ \text{(aminoacyl adenylate formation)} \quad (1)$$

$$\mathrm{aaRS \cdot AA\text{-}AMP} + \mathrm{tRNA} \leftrightarrow \mathrm{AA\text{-}tRNA} + \mathrm{AMP} + \mathrm{aaRS}\ \text{(amino acid transfer to tRNA)} \quad (2)$$

Class I catalytic domains contain a five-stranded parallel β sheet dinucleotide binding (Rossmann) fold and signature sequence motifs HIGH and KMSKS, while class II active sites are built around a seven-stranded antiparallel β sheet with three degenerate sequence motifs (*1*). The class distinctions are maintained across species, with the exception of LysRS,[1] which exists primarily as a class II enzyme but is also found as a class I enzyme in archaea and some bacteria (*4*). Most aaRSs also have additional protein domains that recognize unique tRNA identity elements, facilitate editing of misacylated substrates, or promote protein oligomerization (*5*).

Methionyl-tRNA synthetase (MetRS) is a class I aaRS with a helical bundle anticodon binding domain C-terminal to its catalytic domain (Figure 1A) (*6*). MetRS uses the $tRNA^{Met}$ CAU anticodon as a dominant identity element for aminoacylation (*7*), demonstrating that the consequence of anticodon binding is transmitted ~50 Å to the enzyme active site; the protein component(s) that mediate(s) such intraprotein signaling remain(s) largely unknown. Bridging the anticodon binding and catalytic domains of MetRS is a short structural motif termed the stem contact fold (SCF), based on its structural and positional similarity to a motif in glutaminyl-tRNA synthetase (GlnRS) that contacts the extreme inner corner of its cognate tRNA (*8*, *9*). The SCF is a $\beta-\alpha-\alpha-\beta-\alpha$ domain that contains the class I KMSKS signature sequence on a flexible loop between the first β and α elements of the motif (*10*). Given the location of the SCF between the two functional domains of MetRS, we previously investigated whether it might serve as a flexible hinge to mediate protein conformational change upon cognate tRNA binding, thereby participating in communication between the anticodon binding domain and the catatlytic active site. An engineered disulfide bond that tethered the SCF to the anticodon binding domain decreased anticodon-stimulated tRNA aminoacylation activity under oxidizing conditions; activity was restored upon reduction of the disulfide bond (*11*). In this work, we have further expanded our investigation of the role of the SCF domain in $tRNA^{Met}$ aminoacylation using mutagenic and kinetic analyses.

Comparison of representative class I structures reveals that all members of subclasses Ia and Ib contain an SCF similarly oriented with respect to each protein's Rossmann fold (Figure 1B). Class

†This work was supported by Grant MCB-0448243 from the National Science Foundation and by a fellowship from the National Foundation for Cancer Research to R.W.A.

*To whom correspondence should be addressed: alexanr@wfu.edu (e-mail); 336-758-5568 (phone); 336-758-4656 (fax).

[1]Abbreviations: PP_i, inorganic pyrophosphate; rmsd, root mean squared deviation. Each amino acid is abbreviated using its standard three-letter code.

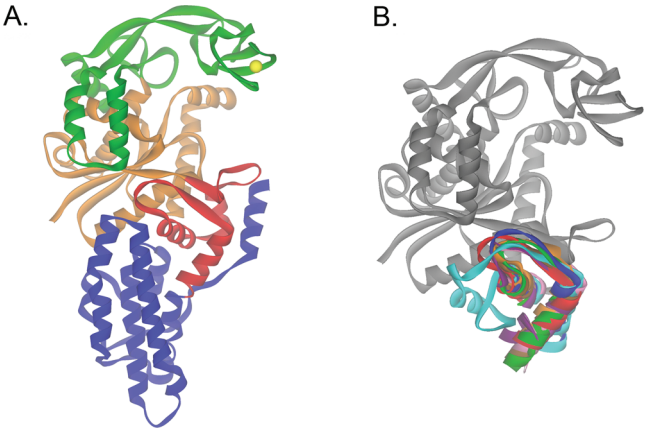

FIGURE 1: Structure of MetRS and the stem contact fold. (A) Structure of monomeric *E. coli* MetRS (residues 3−548; PDB 1QQT (*6*)). The N-terminal catalytic domain includes the class I conserved Rossmann dinucleotide binding fold (orange) bifurcated by the connective polypeptide (CP, green). The SCF (red) is at the interface between the catalytic domain and the helical bundle anticodon binding domain (blue). The zinc ion bound in the CP is a yellow sphere. (B) Alignment of class Ia/Ib aaRS SCF peptides. PDB coordinates were truncated following each protein's SCF peptide and aligned using MultiProt (*30*). The rmsd of the eight proteins was 1.52 Å over 92 Cα atoms of the Rossmann fold and SCF. For clarity, only the MetRS catalytic domain is shown. Aligned proteins are as follows: *E. coli* MetRS (1QQT), red (*6*); *E. coli* GlnRS (1EXD), blue (*31*); *T. thermophilus* LeuRS (1OBH), brown (*32*); *T. thermophilus* GluRS (1N75), cyan (*33*); *E. coli* CysRS (1U0B), pink (*14*); *T. thermophilus* IleRS (1ILE), green (*34*); *T. thermophilus* ArgRS (1IQ0), purple (*15*); and *T. thermophilus* ValRS (1IVS), orange (*35*).

Ib glutamyl-tRNA synthetase (GluRS) is somewhat exceptional among proteins containing the SCF, with an additional short helix inserted within the conserved motif. Class Ic TyrRS and TrpRS, which are obligate dimers and bind their cognate tRNAs across the dimer interface (*12*, *13*), do not contain a structurally analogous SCF domain.

The length of the SCF's first α-helix ranges from 4 residues in CysRS (*14*) to 19 residues in ArgRS (*15*) (DSSP classification (*16*)). For simplicity, we considered here the C-terminal α−β−α region of the SCF, which is composed of two orthogonal helices connected by a tight turn and short β strand. The α−β−α motif occupies a similar position relative to the Rossmann fold domain in class Ia/Ib enzymes, with a Cα rmsd of 1.52 Å over 92 residues of the Rossmann fold and SCF for the aligned structures (Figure 1B). In addition to its presence in the canonical aaRSs, the SCF domain is also present in class I LysRS (*17*) and a synthetase-like *Escherichia coli* enzyme, YadB (*18*).

The SCF sequence similarity across class Ia/Ib aaRSs is low, with only a single arginine residue common among the representative bacterial sequences shown (Figure 2A). This arginine is highly conserved in class Ia enzymes (Arg-356 in *E. coli* MetRS) and is within 3 Å of a highly conserved aspartic acid (Asp-32 in *E. coli* MetRS) positioned within helix αA, which also contains the class I HIGH signature sequence motif. Mutagenesis of MetRS Arg-356 to Gln resulted in an enzyme only 2-fold reduced in tRNA aminoacylation efficiency, indicating that this residue is not a direct contributor to catalytic function (*19*). If the role of the conserved Arg−Asp pair is structural rather than functional, substitution with Gln suggests that a hydrogen bond may serve as a substitute for the presumed electrostatic interaction. While an Arg is similarly positioned in *E. coli* GlnRS and *T. thermophilus* GluRS (Figure 2A), the overall phylogenetic conservation of this residue is much lower in the class Ib enzymes. Likewise, the active site Asp residue is much less conserved in class Ib enzymes, suggesting that this interaction is limited to the class Ia subgroup.

Based on the position of the SCF relative to bound tRNA in complex with representative class Ia/Ib aaRSs, it has been proposed that the SCF motif serves to globally orient an enzyme's cognate tRNA in a non-sequence-specific manner (*10*). Using representative class I cocrystal structures for GlnRS (1O0B) (*20*), CysRS (1U0B) (*14*), ArgRS (2ZUF) (*21*), LeuRS (1WZ2) (*22*), and GluRS (2DXI) (*23*), our LIGPLOT analysis (*24*) revealed that only the GlnRS structure has a base-specific H-bond contact between protein (the Glu-323 carboxylate) and tRNA (the G10 minor groove amino group) (Supporting Information Figure S1). Of the three canonical class I aaRSs that require tRNA for adenylate formation, only GlnRS shows structural evidence of base-specific readout by the SCF motif; analysis of the ArgRS and GluRS cocrystal structures revealed no direct contacts between the SCF and tRNA. This lack of direct readout may be a consequence of subtle variations in tRNA recognition among the enzymes or differences in crystallization conditions (earlier ArgRS and GluRS cocrystal structures revealed two or four, respectively, H-bonds between the SCF and the tRNA backbone). The *Aquifex aeolicus* MetRS:$tRNA^{Met}$ complex (2CSX) is indicative of a pre- or postcatalytic state and does not allow conclusions about catalytically important contacts between the SCF and tRNA core (*25*).

Given the sequence variation and structure conservation of the SCF, we reasoned that we could substitute some residues of one enzyme's motif into another protein context with minimal effect on catalytic activity. We focused on the "loop" region of the SCF that would make a close approach to the tRNA substrate, rather than the portions of the SCF that might be involved in conserved interactions with either the catalytic core or anticodon-binding domain of MetRS. We substituted residues of MetRS's SCF with amino acids of GlnRS that closely approach the inner corner of tRNA (*8*) or with alanines. We also investigated the contribution to MetRS catalytic activity of an aspartic acid residue within the SCF that is common to both MetRS and GlnRS (Figure 2B). We show here that substitutions within the loop of the structurally conserved SCF are tolerated in tRNA aminoacylation, although aminoacyl adenylate formation is impaired. In contrast, substitutions that disrupt contacts between the SCF and the active site are more detrimental to both catalytic steps.

EXPERIMENTAL PROCEDURES

Cloning and Purification of E. coli Methionyl-tRNA Synthetase Variants. The portion of the *metS* gene corresponding to the N-terminal 547 amino acids of *E. coli* MetRS was cloned into pET28 (Novagen) to generate pSW101, which encodes an N-terminally His_6-tagged MetRS monomer (*11*). Mutations were generated in the SCF of *E. coli* MetRS by QuikChange mutagenesis (Stratagene) of pSW101 or its variants. The presence of nucleotide substitutions was confirmed by DNA sequencing. Wild-type and variant proteins were overproduced in BL21-(DE3) cells and purified to homogeneity by nickel affinity chromatography according to the manufacturer's protocol (Qiagen). Proteins were stored in 10 mM Tris-HCl (pH 7.5), 10 mM $MgCl_2$, 10 mM KCl, and 40% glycerol. Protein concentrations were determined by absorbance at 280 nm, with ε_{280} (His_6-MetRS) = 92030 M^{-1} cm^{-1} (*26*).

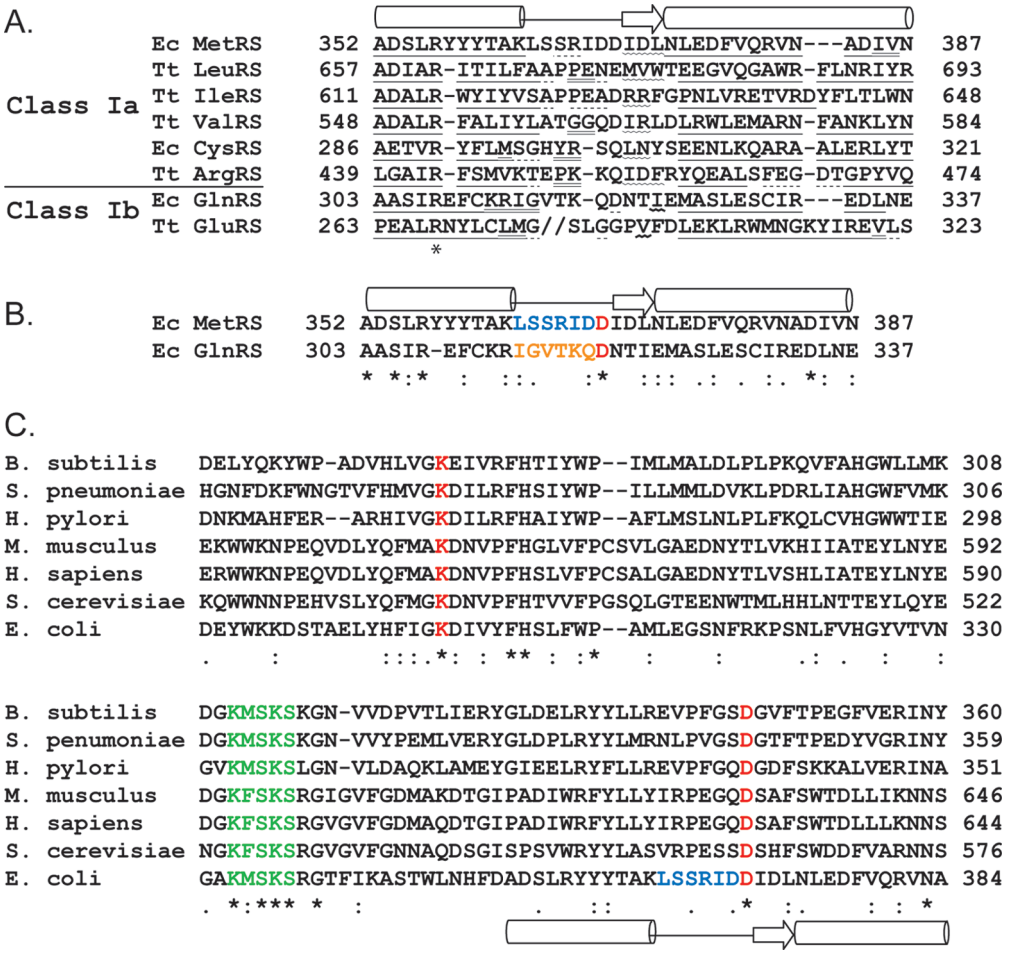

FIGURE 2: Sequence alignment of residues within the SCF. Sequences forming the α−β−α C-terminal portion of the SCF were aligned by ClustalW (*36*). (A) Alignment of class Ia/Ib members. Secondary structure assignments are according to DSSP (*16*). Underline = α helix; bold squiggle underline = residue in isolated β bridge; squiggle underline = extended β strand; double underline = hydrogen-bonded turn; dashed underline = bend. Residues 275−298 of GluRS are omitted in the sequence alignment. (B) Alignment of *E. coli* MetRS and GlnRS sequences. Residues making up the turn of the motif are colored blue (MetRS) or orange (GlnRS). The common aspartic acid at the end of the turn is colored red. Amino acids shared between the two enzymes are colored purple. (C) Alignment of MetRS representatives. The region encompassing the Lys-295 and Glu-369 (*E. coli* numbering) was aligned using ClustalX v.2.0.9 (*37*), and the output was written by ESPript (*38*). The conserved Lys and Glu residues subject to mutagenesis are colored red, the class I KMSKS signature sequence is in green, and the LSSRID sequence subject to substitution is in blue.

Preparation of tRNA. $tRNA^{Met}$ was generated by *in vitro* transcription of BstN1-digested pMET plasmid (*7*) using T7 RNA polymerase, 5 mM each NTP, 10 mM $MgCl_2$, 10 mM DTT, and buffer containing 400 mM Tris-HCl (pH 7.9), 100 mM $MgCl_2$, 50 mM DTT, 0.1% Triton X-100, 50% PEG 8000, 500 μg/mL bovine serum albumin, and 10 mM spermidine at 37 °C for 2−16 h. Transcription products were purified on 8% denaturing polyacrylamide gels and electroeluted using an Elutrap device (Schleicher & Schuell).

Aminoacylation of tRNA. Transfer RNA aminoacylation assays were carried out as described previously (*11*). Transfer RNA^{Met} was annealed by heating to 80 °C in 20 mM HEPES−KOH (pH 7.5), cooling slowly to 60 °C, adding $MgCl_2$ to 1 mM, and then cooling to room temperature. Annealed tRNA (typically 2 μM) was incubated at 25 °C with MetRS (typically 50 nM) in 150 mM NH_4Cl, 20 mM HEPES−KOH (pH 7.5), 10 mM $MgCl_2$, 4 mM ATP, 0.1 mM EDTA, 100 μM methionine, and [^{35}S]methionine (Perkin-Elmer; specific activity >1000 Ci/mmol). Assays to determine kinetic parameters of tRNA aminoacylation were performed at least in duplicate with 100 nM wild-type MetRS and tRNA concentrations ranging from 0.2 to 20 μM $tRNA^{Met}$. For variant proteins, the following enzyme and tRNA concentrations were used: RID → TKQ, RID → AAA, LSSRID → IGVTKQ, and LSSRID → Ala_6, 50 nM enzyme and 0.2−20 μM tRNA; D369A and D369N, 500 nM enzyme and 0.2−40 μM tRNA; K295A and K295V, 500 nM enzyme and 0.5−50 μM tRNA; and D369K/K295D, 500 nM enzyme and 0.2−20 μM tRNA. Methionine and ATP concentrations were held invariant at saturating levels. As higher concentrations of enzyme were required in several cases to generate quantifiable results, K_M data are reported as apparent constants ($K_{M\text{-app}}$). Kinetic parameters were generated from hyperbolic fits of initial velocity of tRNA aminoacylation versus $tRNA^{Met}$ concentration using Origin 8.0 (OriginLab Corp.).

Methionyl Adenylate Assay. Enzyme-catalyzed formation of methionyl adenylate was monitored in a ^{32}P-PP_i−ATP exchange assay as described previously, with ^{32}P-PP_i from Perkin-Elmer as tetrasodium pyrophosphate (specific activity 1−60 Ci/mmol) (*11*). Wild-type MetRS and SCF variants were assayed at 25 °C using 50 nM enzyme, 100 μM methionine, and 2 mM ATP. Assays to determine kinetic parameters of methionyl adenylate formation were performed at least in duplicate with wild-type MetRS at 100 nM and methionine concentrations of 3−300 μM or ATP concentrations of 0.1−4 mM. For variant proteins, the following concentrations were used to determine kinetic parameters: RID → TKQ, RID → AAA, and LSSRID → IGVTKQ,

500 nM enzyme, 3−300 μM methionine, 0.1−6 mM ATP; LSSRID → Ala_6, 500 nM enzyme, 3−500 μM methionine, 0.1−6 mM ATP; D369N, K295A, and K295V, 500 nM enzyme, 3−300 μM methionine, 0.1−4 mM ATP; D369A, 1 μM enzyme, 3−300 μM methionine, 0.1−4 mM ATP; and D369K/K295D, 2 μM enzyme, 2−500 μM methionine, and 0.25−10 μM ATP. Kinetic constants were determined as described for the tRNA aminoacylation assays above.

RESULTS

Construction of MetRS Variants. We used PCR-based mutagenesis to introduce residues of the GlnRS SCF within the structurally similar MetRS domain. In the cocrystal structure of the class Ib *E. coli* GlnRS:$tRNA^{Gln}$, the tetrapeptide ^{316}Thr-Lys-Gln-Asp^{319} (TKQD) forms the closest approach to the extreme inside corner of $tRNA^{Gln}$ (*8*). From structure and sequence alignments, residues ^{366}Arg-Ile-Asp-Asp^{369} (RIDD) of *E. coli* MetRS are proposed to occupy a similar position with respect to $tRNA^{Met}$ (ref *9* and Figure 2). We therefore initiated domain-swapping experiments by replacing the MetRS RID tripeptide with TKQ of the GlnRS sequence (RID → TKQ). We also substituted the RID sequence with alanines (RID → AAA) and replaced six residues of the MetRS loop motif with the corresponding GlnRS residues (^{363}LSSRID^{368} → IGVTKQ) or with alanines (LSSRID → Ala_6). In parallel with construction of these mutations, we evaluated the impact of our most extensive planned peptide swap (replacement of MetRS ^{363}LSSRID^{368} with GlnRS ^{313}IVGTKQ^{318}) *in silico*. While the structural similarity of MetRS and GlnRS is limited to the catalytic domain Rossmann fold and SCF motifs (Supporting Information Figure S2), *in silico* replacement of MetRS ^{363}LSSRID^{368} with GlnRS ^{313}IVGTKQ^{318} followed by energy minimization did not disrupt the MetRS structure (Cα rmsd over 546 residues is 0.04 Å, Supporting Information Figure S3). This result encouraged us to move forward with experimental analyses of all planned mutations. Each of these MetRS variants was expressed and purified to homogeneity by Ni^{2+}-affinity chromatography in the same manner as wild-type MetRS. The ability to obtain soluble purified protein suggested that the variants were stably structured despite the extent of substitutions made, although the solubility was somewhat reduced for the Ala_6 and IGVTKQ variants. In contrast, we swapped the portion of the GlnRS gene encoding the entire α−β−α motif for the corresponding residues of MetRS (36 residues, Figure 2B), which produced an insoluble protein under all growth conditions tested to date (data not shown).

Adjacent to the MetRS loop motif ^{363}LSSRID^{368}, which we replaced with the corresponding GlnRS sequence, is the highly conserved (in MetRS) Asp-369. The carboxylate side chain of Asp-369 is in close proximity to Lys-295, with the lysine amine nitrogen 3.14 Å from the proximal aspartate carboxylate oxygen (*6*). These two residues flank the KMSKS class I signature sequence (Figure 2C) and span the active site and stem contact fold domain. Given the high conservation of these residues and the proximity of their functional groups, we hypothesized that they form an electrostatic interaction or "salt bridge" between the two domains. In order to test the contribution of these residues to MetRS function, variants Asp-369 → Ala (D369A), Asp-369 → Asn (D369N), Lys-295 → Ala (K295A), and Lys-295 → Val (K295V) were generated by QuikChange mutagenesis of parent plasmid pSW101. The doubly substituted Asp-369 → Lys/Lys-295 → Asp (D369K/K295D) was also engineered to determine whether reversed polarity of the presumed electrostatic interaction would promote catalysis. Single or double substitutions were easily obtainable through the same expression and purification procedures used for wild-type MetRS.

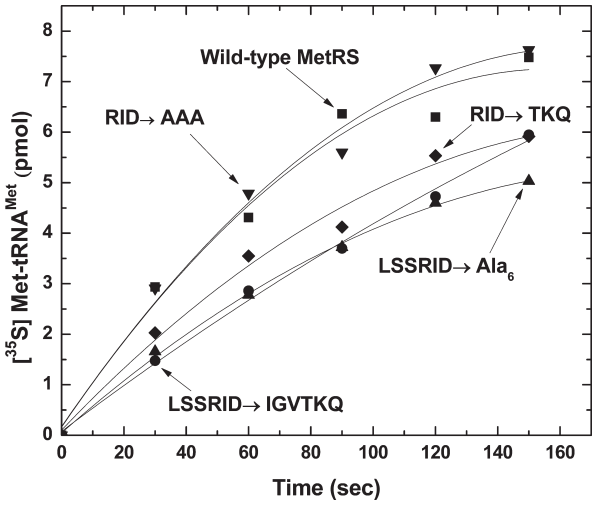

FIGURE 3: Aminoacylation of $tRNA^{Met}$ by MetRS variants. $tRNA^{Met}$ (2 μM) was aminoacylated by 50 nM wild-type MetRS or by RID → TKQ, RID → AAA, LSSRID → RIDTKQ, or LSSRID → $(Ala)_6$ variants. Assays were carried out at 25 °C in 20 mM HEPES−KOH (pH 7.5), 4 mM ATP, 150 mM NH_4Cl, 0.1 mM EDTA, 10 mM $MgCl_2$, 0.1 mM methionine, and [^{35}S]methionine.

Effects of Short Peptide Swaps within the SCF. We investigated the catalytic activity of RID → TKQ, RID → AAA, LSSRID → IGVTKQ, and LSSRID → Ala_6 MetRS variants in tRNA aminoacylation and methionyl adenylate formation. All substitutions of MetRS residues at the first turn of the α−β−α motif resulted in proteins still able to aminoacylate $tRNA^{Met}$ (Figure 3). Even the LSSRID → IGVTKQ and LSSRID → Ala_6 variants displayed only modest reductions in aminoacylation activity. Comparisons of the steady-state kinetic constants for the aminoacylation reaction indicate that a small decrease in k_{cat} is compensated by a corresponding decrease in $K_{M\text{-}app}$ for tRNA (Table 1). The values observed here for wild-type MetRS are consistent with kinetic constants determined earlier for aminoacylation of $tRNA^{fMet}$ at 25 °C by *E. coli* monomeric His_6-MetRS (*27*).

As the first turn of the α−β−α motif is solvent exposed and approximately 10 Å away from MetRS's catalytic active site, we anticipated that methionyl adenylate formation would not be impacted by the mutations made here. Surprisingly, the adenylate synthesis activity of MetRS is much more sensitive to substitutions in the SCF than is the net aminoacylation reaction (Figure 4 and Table 2). The only significant effect on methionine binding occurs for the LSSRID → $(Ala)_6$ variant, for which the methionine $K_{M\text{-}app}$ is increased approximately 3-fold. In contrast, the ATP $K_{M\text{-}app}$ values increase 3−5-fold for all peptide-swapped variants. A decrease in k_{cat} of approximately 6-fold is observed for all variants.

Effects of Mutations at Asp-369 and Lys-295. The ability of MetRS variants D369A, D369N, K295A, and K295V to catalyze methionyl adenylate formation and tRNA aminoacylation was monitored as for the SCF substitutions described above. Transfer RNA aminoacylation was decreased for all variants. Substitutions at Asp-369 are the most detrimental to amino acid transfer (Figure 5 and Table 1), with up to a 125-fold loss in $tRNA^{Met}$ aminoacylation efficiency (k_{cat}/K_M) upon introduction of alanine at this conserved residue. Substitution of the aspartate carboxylate group with an asparagine carboxamide results in a 60-fold loss (Table 1). Removal of the conserved Lys-295 side

Table 1: Steady-State Kinetic Parameters for $tRNA^{Met}$ Aminoacylation[a]

	$K_{M\text{-app}}$(tRNA), μM	k_{cat}, s^{-1}	k_{cat}/K_M, $\mu M^{-1}\cdot s^{-1}$	relative efficiency
wild type	3.9 ± 0.5	1.0 ± 0.2	0.25	1
RID → TKQ	1.4 ± 0.8	0.3 ± 0.2	0.21	0.84
RID → AAA	1.5 ± 0.3	0.4 ± 0.2	0.27	1.1
LSSRID → IGVTKQ	1.2 ± 0.1	0.2 ± 0.1	0.17	0.68
LSSRID → Ala_6	2.5 ± 0.5	0.4 ± 0.1	0.16	0.64
D369A	18 ± 1	0.037 ± 0.004	0.002	0.008
D369N	26 ± 4	0.11 ± 0.01	0.004	0.016
K295A	10.2 ± 0.3	0.042 ± 0.008	0.004	0.016
K295V	17.7 ± 0.5	0.3 ± 0.1	0.017	0.068
D369K/K295D	6 ± 3	0.05 ± 0.01	0.008	0.032

[a]Enzymes were assayed at 100 nM (wild-type MetRS), 50 nM (peptide-swapped variants), or 500 nM (all other variants), with concentrations of tRNA as given in Experimental Procedures. Kinetic parameters were determined by nonlinear curve fitting using Origin 8.0 (OriginLab Corp.). Errors for $K_{M\text{-app}}$ and k_{cat} are standard deviations of two to four measurements.

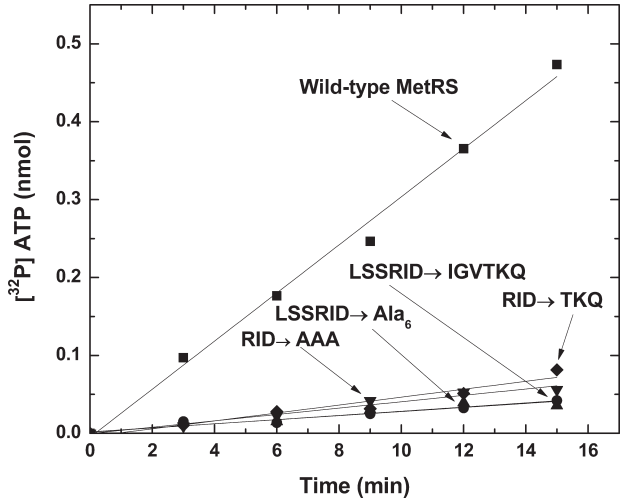

FIGURE 4: Enzyme-catalyzed pyrophosphate exchange. Conversion of [γ-^{32}P]ATP from [^{32}P]pyrophosphate was initiated by 50 nM wild-type MetRS or by RID → TKQ, RID → AAA, LSSRID → RIDTKQ, or LSSRID → $(Ala)_6$ variants. Assays were carried out at 25 °C in 100 mM Tris-HCl (pH 7.5), 10 mM KF, 5 mM $MgCl_2$, 2 mM ATP, 0.1 mg/mL BSA, 0.1 mM methionine, 7 mM 2-mercaptoethanol, 2 mM $NaPP_i$, and ^{32}P-$NaPP_i$.

chain to generate K295A results in a 60-fold loss in aminoacylation efficiency; substitution with valine is less detrimental (loss of only 15-fold). At each position, the $K_{M\text{-app}}$ for $tRNA^{Met}$ is similarly increased whether the substitution is alanine or a larger residue; however, the decrease in k_{cat} for each alanine variant is more striking (Table 1).

Methionyl adenylate formation was also decreased for each of the Asp-369 and Lys-295 substitutions tested (Figure 6). The four variants (D369A, D369N, K295A, and K295V) exhibited a range of methionine activation efficiency, unlike the SCF variants, which were all dramatically impaired in adenylate synthesis (Figure 4). Methionine and ATP $K_{M\text{-app}}$ values were within 2-fold of the wild-type values for D396A and D369N, while the $K_{M\text{-app}}$ values for methionine and ATP were more significantly affected for K295V and K259A, respectively (Table 2). All variants exhibited a decreased catalytic rate constant k_{cat}.

Restoring an Electrostatic Interaction by Compensatory Mutagenesis. The doubly substituted D369K/K295D variant was constructed in an attempt to regenerate an electrostatic interaction between the catalytic and SCF domains. Some gain of function was achieved for tRNA aminoacylation activity relative to the D369A and K295A substitutions (Figure 5); this is due to an improvement in tRNA $K_{M\text{-app}}$ for the double substitution compared to the single alanine variants (Table 1). Despite the enhancement in tRNA aminoacylation, methionyl adenylate synthesis activity was not improved for D369K/K295D relative to the least efficient D369A variant (Figure 6).

Table 2: Steady-State Kinetic Parameters for MetRS-Catalyzed Pyrophosphate Exchange[a]

	$K_{M\text{-app}}$(Met), μM	$K_{M\text{-app}}$(ATP), mM	k_{cat}, s^{-1}
wild type	40 ± 16	0.35 ± 0.05	5.7 ± 0.9
RID → TKQ	26 ± 14	1.4 ± 0.5	0.9 ± 0.3
RID → AAA	48 ± 16	1.15 ± 0.01	1.2 ± 0.2
LSSRID → IGVTKQ	49 ± 1	1.9 ± 0.4	0.9 ± 0.1
LSSRID → Ala_6	128 ± 28	1.6 ± 0.4	1.5 ± 0.5
D369A	37 ± 6	0.8 ± 0.4	0.3 ± 0.1
D369N	19 ± 0.2	0.4 ± 0.1	1.3 ± 0.4
K295A	116 ± 30	1.0 ± 0.1	2.08 ± 0.08
K295V	59 ± 16	1.5 ± 0.3	1.2 ± 0.2
D369K/K295D	94 ± 5	3.2 ± 0.5	0.14 ± 0.04

[a]Enzymes were assayed at 100 nM (wild-type MetRS), 1 μM (D369A), 2 μM (D369K/K295V), or 500 nM (all other variants), with concentrations of ATP and methionine as given in Experimental Procedures. Kinetic parameters were determined by nonlinear curve fitting using Origin 8.0 (OriginLab Corp.). k_{cat} values represent the average of all determinations at saturating ATP or methionine. Errors for $K_{M\text{-app}}$ are standard deviations of two to three measurements, while errors for k_{cat} are standard deviations of four to six measurements.

DISCUSSION

Substitutions of the SCF Loop Affect Adenylate Formation. Given the surface position of the SCF loop where substitutions were made, we anticipated that substitutions would either have no effect on MetRS catalysis or might impact productive tRNA binding (reflected by an increase in $K_{M\text{-app}}$), resulting in decreased catalytic efficiency for the net aminoacylation reaction. The dramatic effect of SCF substitutions on methionyl adenylate formation despite relatively robust $tRNA^{Met}$ aminoacylation was thus surprising. The effects on substrate binding are likely to be indirect, as Ile-367 in the turn of the $\alpha-\beta-\alpha$ motif is 9.5 Å from ATP bound in the enzyme active site and 14.5 Å from bound methionine (*28*). For example, substitution of amino acids in the turn of the motif may alter the conformation of the subsequent β strand (^{360}IDL^{362}), which interacts with the first β strand of the SCF $\beta-\alpha-\alpha-\beta-\alpha$ domain. Intradomain hydrogen bonding and electrostatic interactions no doubt contribute to the overall

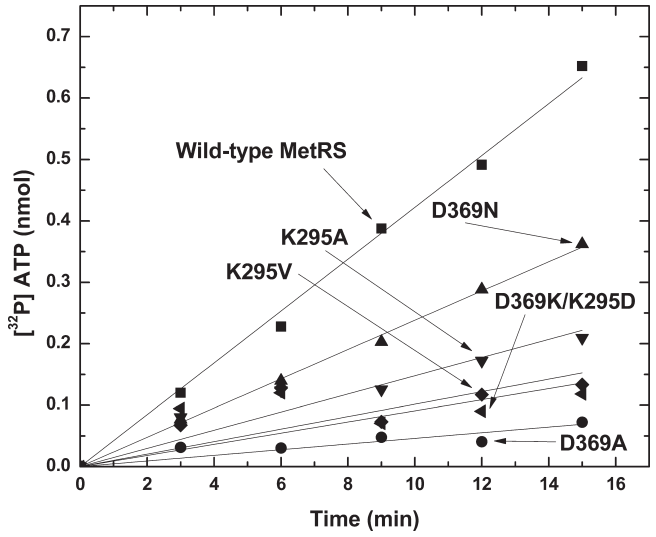

FIGURE 5: Aminoacylation of $tRNA^{Met}$ by MetRS variants. $tRNA^{Met}$ (2 μM) was aminoacylated by 50 nM wild-type MetRS or D369A, D369N, K295A, K295V, or D369K/K295D variants. Assays were carried out at 25 °C in 20 mM HEPES−KOH (pH 7.5), 4 mM ATP, 150 mM NH_4Cl, 0.1 mM EDTA, 10 mM $MgCl_2$, 0.1 mM methionine, and [^{35}S]methionine.

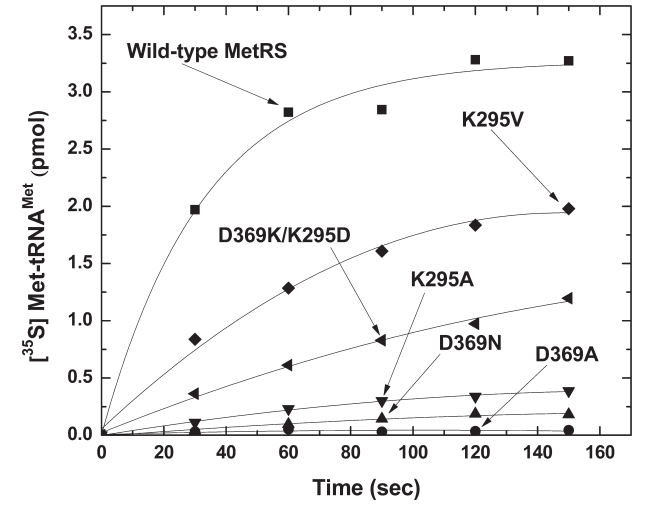

FIGURE 6: Enzyme-catalyzed pyrophosphate exchange. Conversion of [γ-^{32}P]ATP from [^{32}P]pyrophosphate was initiated by 50 nM wild-type MetRS or D369A, D369N, K295A, K295V, or D369K/K295D variants. Assays were carried out at 25 °C in 100 mM Tris-HCl (pH 7.5), 10 mM KF, 5 mM $MgCl_2$, 2 mM ATP, 0.1 mg/mL BSA, 0.1 mM methionine, 7 mM 2-mercaptoethanol, 2 mM $NaPP_i$, and ^{32}P-$NaPP_i$.

stability of the domain, such that amino acid substitutions, even at solvent-exposed turns, may subtly affect the overall conformation of this critical region of MetRS. Nevertheless, the ability of turn variants to support $tRNA^{Met}$ aminoacylation is consistent with the previously proposed role for the SCF as a structural platform for orienting the tRNA on the protein surface.

As the SCF variants affected the efficiency of tRNA-independent methionyl adenylate formation but not tRNA aminoacylation (which encompasses adenylate formation and amino acid transfer, as well as product release), we investigated whether the SCF variants became tRNA-dependent for methionyl adenylate formation. Such a mechanistic change would be particularly noteworthy, as the IGVTKQ sequence used is from GlnRS, an enzyme that does require tRNA binding for amino acid activation. Under

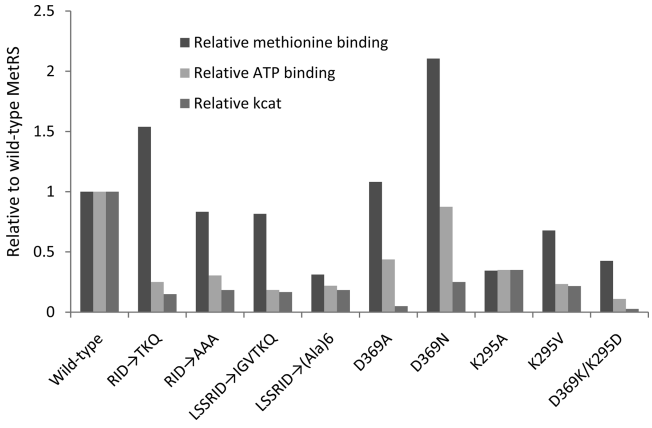

FIGURE 7: Summary of methionyl adenylate kinetic parameters. Normalized (relative to wild-type MetRS) kinetic parameters are shown for each of the variants described in the text. Relative values for k_{cat} are k_{cat}(variant)/k_{cat}(wild type), while relative binding is determined as $K_{M\text{-}app}$(wild type)/$K_{M\text{-}app}$(variant) to graphically indicate the inverse relationship between the Michaelis constant and productive substrate binding.

steady-state conditions no enhancement of adenylate formation occurred for any of the SCF variants when pyrophosphate exchange assays were conducted either in the presence of oxidized $tRNA^{Met}$ or in the presence of untreated $tRNA^{Met}$ at low pH (data not shown). [Decreased reaction pH has been shown to slow the rate of amino acid transfer without affecting aminoacyl adenylate formation (*29*).] While the variants did not become tRNA dependent for adenylate synthesis, some coupling between tRNA binding and efficient amino acid activation may be occurring. In order to determine whether substitutions in the SCF affect elementary catalytic rates for adenylate synthesis, amino acid transfer, or product release, rapid chemical quench kinetics will be necessary to determine pre-steady-state kinetic parameters.

Conserved Residues Lys-295 and Asp-369 Cannot Be Swapped. Functional assays make it clear that mutation at either Lys-295 or Asp-369 reduces catalytic activity of MetRS (Figures 5 and 6). Apparent kinetic constants for these variants (determined at elevated enzyme concentration) indicate that k_{cat} of adenylate formation is more impacted for Asp-369 substitutions, while $K_{M\text{-}app}$ values for ATP and methionine are more affected for Lys-295 variants (Figure 7). While neither residue makes direct contact with ATP or methionine in the enzyme active site, Lys-295 is in closer proximity to these small molecule substrates, with the adjacent Gly-294 backbone making H-bond contact with an ATP ribose hydroxyl group (*28*). The impact on adenylate formation of substitution at Asp-369 is likely to be due to a general disruption of the active site structure, as for other SCF variants described above. Both Lys-295 and Asp-369 are highly conserved, suggesting that contacts between them and with other residues in the vicinity are important for structural and functional integrity of the protein. The simple swap of these residues restored aminoacylation activity only modestly compared to the most impaired variants (Figure 5), likely because the proposed Lys−Asp electrostatic contact occurs in the context of other H-bonding and hydrophobic interactions. For example, the Lys-295 ε-amino group is in hydrogen bond distance to the amide oxygen of Ile-367, and the Asp-369 carboxylate makes close contact with the amide proton of Tyr-325. Thus even if the K295D/D369K variant retained the electrostatic interaction of the wild-type enzyme, other contacts were lost, disrupting the fine-tuned structure between the active site and SCF.

CONCLUSION

In the absence of a MetRS:tRNA^{Met} cocrystal structure that would reveal specific contacts between the SCF and tRNA core, it is difficult to determine precisely how the SCF variants described here affect methionyl adenylate formation despite their distance from the MetRS active site. Nevertheless, we can conclude that any contribution to tRNA recognition by the class Ia/Ib SCF motif occurs in a structure-dependent rather than sequence-dependent manner.

ACKNOWLEDGMENT

The authors thank Zack Denton for technical assistance.

SUPPORTING INFORMATION AVAILABLE

Supplementary figures and experimental procedures pertaining to structural comparison of *E. coli* GlnRS and MetRS and *in silico* mutagenesis of MetRS. This material is available free of charge via the Internet at http://pubs.acs.org.

REFERENCES

1. Ibba, M., and Söll, D. (2000) Aminoacyl-tRNA synthesis. *Annu. Rev. Biochem. 69*, 617–650.
2. Cusack, S., Berthet-Colominas, C., Hartlein, M., Nassar, N., and Leberman, R. (1990) A second class of synthetase structure revealed by X-ray analysis of *Escherichia coli* seryl-tRNA synthetase at 2.5 Å. *Nature 347*, 249–255.
3. Eriani, G., Delarue, M., Poch, O., Gangloff, J., and Moras, D. (1990) Partition of tRNA synthetases into two classes based on mutually exclusive sets of sequence motifs. *Nature 347*, 203–206.
4. Ibba, M., Morgan, S., Curnow, A. W., Pridmore, D. R., Vothknecht, U. C., Gardner, W., Lin, W., Woese, C. R., and Söll, D. (1997) A euryarchaeal lysyl-tRNA synthetase: resemblance to class I synthetases. *Science 278*, 1119–1122.
5. Alexander, R. W., and Schimmel, P. (2001) Domain-domain communication in aminoacyl-tRNA synthetases. *Prog. Nucleic Acid Res. Mol. Biol. 69*, 317–349.
6. Mechulam, Y., Schmitt, E., Maveyraud, L., Zelwer, C., Nureki, O., Yokoyama, S., Konno, M., and Blanquet, S. (1999) Crystal structure of *Escherichia coli* methionyl-tRNA synthetase highlights species-specific features. *J. Mol. Biol. 294*, 1287–1297.
7. Schulman, L. H., and Pelka, H. (1988) Anticodon switching changes the identity of methionine and valine transfer RNAs. *Science 242*, 765–768.
8. Rould, M. A., Perona, J. J., Söll, D., and Steitz, T. A. (1989) Structure of *E. coli* glutaminyl-tRNA synthetase complexed with tRNA(Gln) and ATP at 2.8 Å resolution. *Science 246*, 1135–1142.
9. Perona, J. J., Rould, M. A., Steitz, T. A., Risler, J. L., Zelwer, C., and Brunie, S. (1991) Structural similarities in glutaminyl- and methionyl-tRNA synthetases suggest a common overall orientation of tRNA binding. *Proc. Natl. Acad. Sci. U.S.A. 88*, 2903–2907.
10. Sugiura, I., Nureki, O., Ugaji-Yoshikawa, Y., Kuwabara, S., Shimada, A., Tateno, M., Lorber, B., Giege, R., Moras, D., Yokoyama, S., and Konno, M. (2000) The 2.0 Å crystal structure of *Thermus thermophilus* methionyl-tRNA synthetase reveals two RNA-binding modules. *Structure 8*, 197–208.
11. Banerjee, P., Warf, M. B., and Alexander, R. (2009) Effect of a domain-spanning disulfide on aminoacyl-tRNA synthetase activity. *Biochemistry 48*, 10113–10119.
12. Yang, X. L., Otero, F. J., Ewalt, K. L., Liu, J., Swairjo, M. A., Kohrer, C., RajBhandary, U. L., Skene, R. J., McRee, D. E., and Schimmel, P. (2006) Two conformations of a crystalline human tRNA synthetase-tRNA complex: implications for protein synthesis. *EMBO J. 25*, 2919–2929.
13. Yaremchuk, A., Kriklivyi, I., Tukalo, M., and Cusack, S. (2002) Class I tyrosyl-tRNA synthetase has a class II mode of cognate tRNA recognition. *EMBO J. 21*, 3829–3840.
14. Hauenstein, S., Zhang, C. M., Hou, Y. M., and Perona, J. J. (2004) Shape-selective RNA recognition by cysteinyl-tRNA synthetase. *Nat. Struct. Mol. Biol. 11*, 1134–1141.
15. Shimada, A., Nureki, O., Goto, M., Takahashi, S., and Yokoyama, S. (2001) Structural and mutational studies of the recognition of the arginine tRNA-specific major identity element, A20, by arginyl-tRNA synthetase. *Proc. Natl. Acad. Sci. U.S.A. 98*, 13537–13542.
16. Kabsch, W., and Sander, C. (1983) Dictionary of protein secondary structure: pattern recognition of hydrogen-bonded and geometrical features. *Biopolymers 22*, 2577–2637.
17. Terada, T., Nureki, O., Ishitani, R., Ambrogelly, A., Ibba, M., Söll, D., and Yokoyama, S. (2002) Functional convergence of two lysyl-tRNA synthetases with unrelated topologies. *Nat. Struct. Biol. 9*, 257–262.
18. Dubois, D. Y., Blaise, M., Becker, H. D., Campanacci, V., Keith, G., Giege, R., Cambillau, C., Lapointe, J., and Kern, D. (2004) An aminoacyl-tRNA synthetase-like protein encoded by the *Escherichia coli* yadB gene glutamylates specifically tRNAAsp. *Proc. Natl. Acad. Sci. U.S.A. 101*, 7530–7535.
19. Ghosh, G., Brunie, S., and Schulman, L. H. (1991) Transition state stabilization by a phylogenetically conserved tyrosine residue in methionyl-tRNA synthetase. *J. Biol. Chem. 266*, 17136–17141.
20. Bullock, T. L., Uter, N., Nissan, T. A., and Perona, J. J. (2003) Amino acid discrimination by a class I aminoacyl-tRNA synthetase specified by negative determinants. *J. Mol. Biol. 328*, 395–408.
21. Konno, M., Sumida, T., Uchikawa, E., Mori, Y., Yanagisawa, T., Sekine, S., and Yokoyama, S. (2009) Modeling of tRNA-assisted mechanism of Arg activation based on a structure of Arg-tRNA synthetase, tRNA, and an ATP analog (ANP). *FEBS J. 276*, 4763–4779.
22. Tukalo, M., Yaremchuk, A., Fukunaga, R., Yokoyama, S., and Cusack, S. (2005) The crystal structure of leucyl-tRNA synthetase complexed with tRNALeu in the post-transfer-editing conformation. *Nat. Struct. Mol. Biol. 12*, 923–930.
23. Sekine, S., Shichiri, M., Bernier, S., Chenevert, R., Lapointe, J., and Yokoyama, S. (2006) Structural bases of transfer RNA-dependent amino acid recognition and activation by glutamyl-tRNA synthetase. *Structure 14*, 1791–1799.
24. Wallace, A. C., Laskowski, R. A., and Thornton, J. M. (1995) LIGPLOT: a program to generate schematic diagrams of protein-ligand interactions. *Protein Eng. 8*, 127–134.
25. Nakanishi, K., Ogiso, Y., Nakama, T., Fukai, S., and Nureki, O. (2005) Structural basis for anticodon recognition by methionyl-tRNA synthetase. *Nat. Struct. Mol. Biol. 12*, 931–932.
26. Gasteiger, E., Gattiker, A., Hoogland, C., Ivanyi, I., Appel, R. D., and Bairoch, A. (2003) ExPASy: the proteomics server for in-depth protein knowledge and analysis. *Nucleic Acids Res. 31*, 3784–3788.
27. Alexander, R. W., and Schimmel, P. (1999) Evidence for breaking domain-domain functional communication in a synthetase-tRNA complex. *Biochemistry 38*, 16359–16365.
28. Crepin, T., Schmitt, E., Mechulam, Y., Sampson, P. B., Vaughan, M. D., Honek, J. F., and Blanquet, S. (2003) Use of analogues of methionine and methionyl adenylate to sample conformational changes during catalysis in *Escherichia coli* methionyl-tRNA synthetase. *J. Mol. Biol. 332*, 59–72.
29. Uter, N. T., Gruic-Sovulj, I., and Perona, J. J. (2005) Amino acid-dependent transfer RNA affinity in a class I aminoacyl-tRNA synthetase. *J. Biol. Chem. 280*, 23966–23977.
30. Shatsky, M., Nussinov, R., and Wolfson, H. J. (2004) A method for simultaneous alignment of multiple protein structures. *Proteins 56*, 143–156.
31. Bullock, T. L., Sherlin, L. D., and Perona, J. J. (2000) Tertiary core rearrangements in a tight binding transfer RNA aptamer. *Nat. Struct. Biol. 7*, 497–504.
32. Lincecum, T. L., Jr., Tukalo, M., Yaremchuk, A., Mursinna, R. S., Williams, A. M., Sproat, B. S., Van Den Eynde, W., Link, A., Van Calenbergh, S., Grotli, M., Martinis, S. A., and Cusack, S. (2003) Structural and mechanistic basis of pre- and posttransfer editing by leucyl-tRNA synthetase. *Mol. Cell 11*, 951–963.
33. Sekine, S., Nureki, O., Dubois, D. Y., Bernier, S., Chenevert, R., Lapointe, J., Vassylyev, D. G., and Yokoyama, S. (2003) ATP binding by glutamyl-tRNA synthetase is switched to the productive mode by tRNA binding. *EMBO J. 22*, 676–688.
34. Nureki, O., Vassylyev, D. G., Tateno, M., Shimada, A., Nakama, T., Fukai, S., Konno, M., Hendrickson, T. L., Schimmel, P., and Yokoyama, S. (1998) Enzyme structure with two catalytic sites for double-sieve selection of substrate. *Science 280*, 578–582.
35. Fukai, S., Nureki, O., Sekine, S., Shimada, A., Vassylyev, D. G., and Yokoyama, S. (2003) Mechanism of molecular interactions for tRNA(Val) recognition by valyl-tRNA synthetase. *RNA 9*, 100–111.
36. Thompson, J. D., Higgins, D. G., and Gibson, T. J. (1994) CLUSTAL W: improving the sensitivity of progressive multiple sequence alignment through sequence weighting, position-specific gap penalties and weight matrix choice. *Nucleic Acids Res. 22*, 4673–4680.
37. Larkin, M. A., Blackshields, G., Brown, N. P., Chenna, R., McGettigan, P. A., McWilliam, H., Valentin, F., Wallace, I. M., Wilm, A., Lopez, R., Thompson, J. D., Gibson, T. J., and Higgins, D. G. (2007) Clustal W and Clustal X version 2.0. *Bioinformatics 23*, 2947–2948.
38. Gouet, P., Courcelle, E., Stuart, D. I., and Metoz, F. (1999) ESPript: analysis of multiple sequence alignments in PostScript. *Bioinformatics 15*, 305–308.